The [Lys^{-2}-Arg^{-1}-des(17−21)]-Endothelin-1 Peptide Retains the Specific Arg^{-1}−Asp^{8} Salt Bridge but Reveals Discrepancies between NMR Data and Molecular Dynamics Simulations†

Quentin Kaas,‡ André Aumelas,*,‡ Shigeru Kubo,§ Naoyoshi Chino,§ Yuji Kobayashi,|| and Laurent Chiche*,‡

Centre de Biochimie Structurale, UMR5048 CNRS-Université Montpellier I, UMR554 INSERM-Université Montpellier I, Faculté de Pharmacie, 15 avenue Charles Flahault, BP 14491, 34093 Montpellier-Cedex 5, France, Peptide Institute, Inc., Osaka, Japan, and Institute for Protein Research and Faculty of Pharmaceutical Sciences, Osaka University, Osaka, Japan

Received February 27, 2002; Revised Manuscript Received May 23, 2002

ABSTRACT: The [des(17−21)]-endothelin-1 (CSH-ET) and [Lys^{-2}-Arg^{-1}-des(17−21)]-endothelin-1 (KR-CSH-ET) peptides, designed by removing the five-residue hydrophobic tail from the endothelin-1 (ET-1) and [Lys^{-2}-Arg^{-1}]-endothelin-1 (KR-ET-1) peptides, respectively, were synthesized. Previous studies on KR-ET-1 showed that, in contrast to ET-1, this engineered compound displays a pH-dependent conformational change related to the formation of a stabilizing salt bridge between the Arg^{-1} and Asp^{8} side chains. CD and NMR spectra indicate that CSH-ET and KR-CSH-ET display conformational behavior similar to those of ET-1 and KR-ET-1, respectively. The short salt bridge-stabilized KR-CSH-ET peptide therefore appears to be an attractive elementary scaffold for drug design. The solution structure of the salt-bridged form of KR-CSH-ET was determined by NMR at pH 4.5 and is very similar to the corresponding form of the parent KR-ET-1 peptide. Molecular dynamics simulations of the salt-bridged form of KR-CSH-ET were performed using both the GB/SA implicit solvation scheme or an explicit solvation and the particle-mesh Ewald method for long-range electrostatic calculation. Unexpectedly, the Arg^{-1}−Asp^{8} salt bridge does not display in the simulation the stability that could be expected from the experimental data. The cooperative involvement of a cation−π interaction in formation of the salt bridge has been hypothesized. Difficulties in accurately simulating cation−π interactions might be responsible for the lack of stability in the simulation. At this time, however, no definitive explanation for the observed discrepancy between experiments and simulations is available, and further experimental studies appear to be necessary to fully understand in atomic detail the pH-dependent conformational change observed in the KR-ET-1 series.

The [Lys^{-2}−Arg^{-1}]-endothelin-1 peptide (KR-ET-1)[1] resulting from the N-terminal addition of the KR dipeptide of the ET-1 pro sequence to ET-1 (Figure 1) showed improved formation of native disulfide bridges, but decreased contractile activity (*1*−*3*). NMR structural studies of KR-ET-1 indicated that KR-ET-1 undergoes a pH-dependent conformational modification with formation of a salt bridge between Arg^{-1} of the pro sequence and Asp^{8} in the carboxylate state (pH >4). The presence of the salt bridge

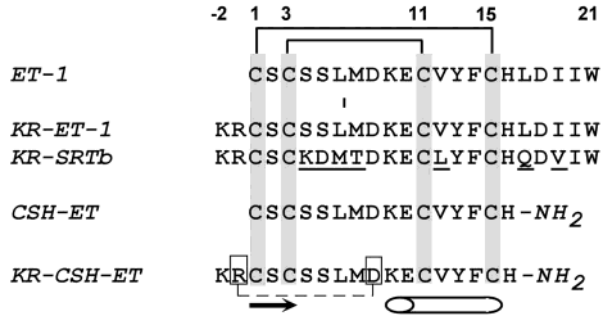

FIGURE 1: Sequences of ET-1, KR-ET-1, and KR-SRTb and of shorter peptides CSH-ET and KR-CSH-ET resulting from C-terminal tail removal in ET-1 and KR-ET-1, respectively. Shaded boxes highlight cysteines, and thick lines represent disulfide bridges. The sequence numbering of ET-1 is used, with negative numbers for the KR dipeptide, and is shown on the top of the sequences. Sequence differences between KR-ET-1 and KR-SRTb are underlined. The Arg^{-1}−Asp^{8} salt bridge is shown as boxes linked with a dashed line for KR-CSH-ET. The arrow and the cylinder at the bottom indicate the location of the short β-strand and the helix, respectively.

† This work was supported by the Centre Informatique National de l'Enseignement Supérieur, Montpellier-Cedex 5, France.

* To whom correspondence should be addressed. Telephone: +33 [0]4 67 04 34 32. Fax: +33 [0]4 67 52 96 23. E-mail: chiche@cbs.cnrs.fr or aumelas@cbs.cnrs.fr.

‡ UMR5048 CNRS-Université Montpellier I and UMR554 INSERM-Université Montpellier I.

§ Peptide Institute, Inc.

|| Osaka University.

[1] Abbreviations: 1D, one-dimensional; 2D, two-dimensional; 3D, three-dimensional; CSH motif, cystine-stabilized helical motif; CSH-ET, [des(17−21)]-endothelin-1; COSY, correlated spectroscopy; ET, endothelin; GB, generalized Born; GSH and GSSG, reduced and oxidized glutathione, respectively; H-bond, hydrogen bond; KR-ET-1, [Lys^{-2}-Arg^{-1}]-endothelin-1; KR-CSH-ET, [Lys^{-2}-Arg^{-1}-des(17−21)]-endothelin-1; NMR, nuclear magnetic resonance; NOE, nuclear Overhauser effect; NOESY, nuclear Overhauser effect spectroscopy; PME, particle-mesh Ewald; rms, root-mean-square; SA, surface area; SD, standard deviation; SRTb, sarafotoxin-S6b; TOCSY, total correlated spectroscopy; TSP-d_4, sodium 2,2,3,3-tetradeuterio-3-(trimethylsilyl)-propionate.

10.1021/bi025744z CCC: $22.00
Published on Web 08/23/2002

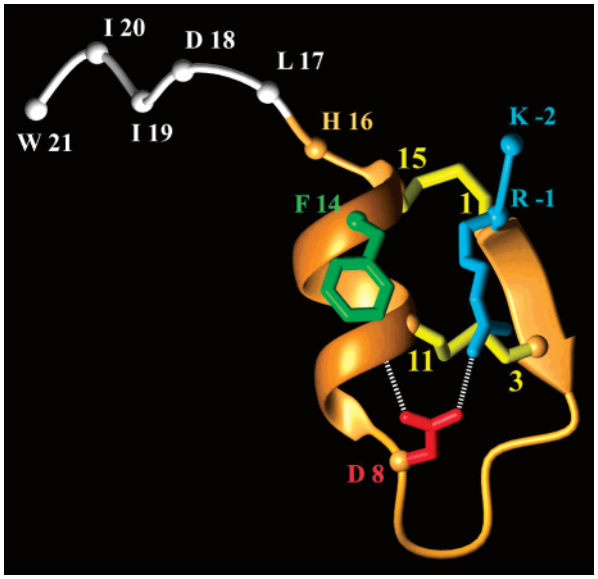

FIGURE 2: Schematic view of the KR-ET-1 structure. The ribbon is colored as follows: orange, elementary CSH motif; blue, Lys-Arg N-terminal extension from the ET-1 pro sequence added in KR-ET-1 and KR-CSH-ET; and white, C-terminal tail removed in CSH-ET and KR-CSH-ET. Cysteine, Arg^{-1}, Asp^{8}, and Phe^{14} side chains are shown as yellow, blue, red, and green sticks, respectively. Hydrogen bonds corresponding to the capping of the helix by Asp^{8} and to the $Arg^{-1}-Asp^{8}$ ionic interaction are shown as dashed white lines.

in KR-ET-1 was deduced from analysis of chemical shift alterations due to pH variation. Overall, the alterations include a larger amide proton chemical range and strong nonequivalence of H^{β} protons of cysteines, indicative of a more rigid conformation in the carboxylate state. The salt bridge is indicated by a large downfield shift of the Arg^{-1} H^{ϵ} signal (*4*). Also typical of the salt-bridged conformation are the strong nonequivalence of the two Arg^{-1} H^{δ} protons and of the two Asp^{8} H^{β} protons and the upfield shift and nonequivalence of the Phe^{14} aromatic protons. The $Arg^{-1}-Asp^{8}$ salt bridge in KR-ET-1 was furthermore confirmed by electrospray mass spectroscopy and by the study of the E10Q, D18N, and D8N analogues (*3*). Direct observation of such Arg−Asp salt bridge by ^{1}H NMR is precluded by the absence of side chain−side chain proximities. It could only be achieved through complex and costly high-level NMR techniques using a ^{13}C and ^{15}N doubly labeled compound (*4*). The stabilization due to formation of the salt bridge was suspected to thermodynamically favor formation of the native disulfide bridges in KR-ET-1.

Interestingly, a similar phenomenon was observed when the KR dipeptide from the ET-1 pro sequence was grafted at the N-terminus of sarafotoxin-S6b, another peptide belonging to the ET family, to give the KR-SRTb chimeric peptide (Figure 1). Both ET-1 and SRT-6b display similar structures composed of the cystine stabilized helical motif (CSH) in which a two-turn helix is linked to a short β-strand by two disulfide bridges (*5*−*7*), and a less well-defined five-residue C-terminal tail (Figure 2). As shown by the sequence differences between KR-ET-1 and KR-SRTb (Figure 1), the $Arg^{-1}-Asp^{8}$ salt bridge remained unaffected by modification of the loop of residues 4−7 and of the C-terminal tail. The salt bridge therefore appeared to be a means of stabilizing the elementary CSH motif with potential applications in drug design and protein engineering (*8*). However, the exact role of the C-terminal tail in salt bridge stabilization remains to be determined.

On the other hand, restrained simulated annealing or short molecular dynamics (MD) simulations performed on the KR-ET-1 or the KR-SRTb peptide structures surprisingly resulted in breakage of the $Arg^{-1}-Asp^{8}$ salt bridge unless additional specific salt bridge constraints were used in the calculations (*1*, *8*). This observation suggested that further work was necessary to better understand the stability of the $Arg^{-1}-Asp^{8}$ salt bridge. We therefore decided to synthesize two shorter peptides in which the hydrophobic C-terminal tail has been removed, and to use these peptides as simpler models to carefully study the conformation and stability of the salt bridge. The short peptides, hereafter called KR-CSH-ET (18 residues) and CSH-ET (16 residues), correspond to the isolated CSH motif, with and without the N-terminal dipeptide extension, respectively (Figure 1). The peptides were amidated at the new C-terminus to avoid introduction of a negative charge at a position where the parent peptides display a peptide bond. Besides its potential interest as an elementary stabilized scaffold for engineering purposes, the KR-CSH-ET peptide constitutes a convenient model for investigation of salt bridge stability in molecular dynamics simulations. Indeed, understanding the structure and the stability of the $Arg^{-1}-Asp^{8}$ salt bridge at the atomic level is of general interest since, although the important role of salt bridges in the conformational stability of proteins is well-recognized, the effect of surface salt bridges remains controversial (*9*−*12*). Our goals in this study were twofold. First, we sought to determine the smallest salt-bridged stabilized CSH motif, and second, we sought to obtain new information about the pH-dependent modification in the KR-ET-1 series.

MATERIALS AND METHODS

Experimental Studies

Synthesis and Oxidative Folding. The CSH-ET and KR-CSH-ET peptides having trityl (Trt) and acetamidomethyl (Acm) groups on Cys residues at different positions were elongated on the solid support applying the standard Fmoc strategy. After cleavage of the peptide from the resin with a trifluoroacetic acid (TFA)/H_2O/thiophenol/triisopropylsilane mixture for 2 h, two disulfide bonds were formed selectively according to the previously described scheme (*13*, *14*).

The oxidative folding of the reduced peptides of CSH-ET and KR-CSH-ET was carried out by the same method reported previously (*13*, *14*). Briefly, the reduced peptide was subjected to the oxidative folding reaction in 0.1 M ammonium acetate buffer at pH 9.5 at a peptide concentration of 0.01 mM and 25 °C. The ratio of the native to the non-native disulfide isomers was determined from the peak areas on RP-HPLC analysis.

Circular Dichroism. CD spectra of CSH-ET and KR-CSH-ET were recorded at 25 °C on a JASCO J720 spectrophotometer using a 1 mm path length cell. Peptide solutions were prepared at a concentration of 0.05 mM, and the spectra were recorded at pH 4.0 and 1.5. Each spectrum was scanned from 190 to 250 nm and accumulated for eight scans.

NMR. Samples were prepared by dissolving lyophilized peptides (1.7 mg) in 0.45 mL of a 95% H_2O/5% $^{2}H_2O$

mixture (v/v). The peptide concentration of the resulting sample was ~1.8 mM, and the pH was adjusted by addition of dilute HCl or NaOH. All ^{1}H NMR spectra were recorded on a Bruker AMX-600 spectrometer, and TSP-d_4 was used as an internal reference. The 1D spectra as a function of pH were acquired at 27 °C with the "Jump and Return" sequence to observe signals of exchangeable protons (*15*). 2D experiments, COSY, TOCSY (80 ms spin lock), and NOESY (150 ms mixing time), were carried out at 7 °C and pH 4.5.

Structure Calculations. Structure calculations were performed on a Silicon Graphics Origin 200 workstation. The structures were displayed and analyzed using either INSIGHT II (MSI, San Diego, CA) on a Silicon Graphics O2 workstation or MOLMOL 2K.1 (*16*) on a Linux box. The NOE intensities were classified as strong, medium, and weak, and converted into distance constraints of 2.5, 3.0, and 4.0 Å, respectively. If the connectivity involved side chain protons, 3.0, 4.0, and 5.0 Å upper bounds, respectively, were used instead to account for higher mobility. For sequential $d_{\alpha N}$ and d_{NN} connectivities, we used upper bounds of 2.5, 3.0, and 3.5 Å and 2.8, 3.3, and 4.0 Å, respectively. When necessary, the distance constraints were corrected for pseudoatoms (*17*). Φ angles of residues with small or large $^3J_{HN-H^\alpha}$ coupling constants (<4 or >8.5 Hz) were constrained in the −90 to −40° or −160 to −80° ranges. χ_1 angles of residues for which stereospecific attribution of the β protons could be achieved were constrained in the corresponding range. Disulfide bridges were imposed through distance constraints of 2.0−2.1, 3.0−3.1, and 3.75−3.95 Å on Si−Sj, Si−Cβj, and Cβi−Cβj distances, respectively. No H-bond was imposed.

3D structures were obtained from the distance and angle restraints using the torsion angle molecular dynamics method available in the DYANA program (*18*). One thousand structures were then calculated with the standard simulated annealing protocol. The 50 structures with the lowest violation of the target function were selected for further refinement. They were submitted to molecular mechanics energy refinement with the SANDER module of the AMBER 6.0 program (*19*), using the all-atom parm94 force field (*20*) and the GB/SA implicit solvation system (*21*−*23*). Pseudoenergy terms taking into account the NMR interproton distance restraints were defined as follows via four threshold distance values: r_1, r_2, r_3, and r_4. In all cases, r_1 and r_2 were set to 1.3 and 1.8 Å, respectively. r_3 was taken to be the upper boundary used in the DYANA calculations, and r_4 was chosen as r_3 + 0.5 Å. For an observed distance lying between r_2 and r_3, no restraint was applied. Between r_1 and r_2 or between r_3 and r_4, parabolic restraints were applied. Outside the r_1−r_4 range, the restraints were linear with slopes identical to parabolic slopes at points r_1 and r_4. A similar strategy was used for dihedral restraints. When no stereospecific assignment could be achieved for methyl or methylene protons, an $\langle r^{-6}\rangle^{-1/6}$ averaging scheme was used instead of pseudoatoms. Five thousand cycles of restrained energy minimization were first carried out followed by a 30 ps long simulated annealing procedure in which the temperature was raised to 900 K for 20 ps and then gradually lowered to 300 K. During this stage, the force constants for the NMR distance and dihedral constraints were gradually increased from 3.2 to 32 kcal mol^{-1} Å^{-2} and from 0.5 to 50 kcal mol^{-1} rad^{-2}, respectively.

Figures of structures were produced with the MOLMOL (*16*) and POV-Ray (http://www.povray.org) programs.

Molecular Dynamics Simulations

All molecular dynamics runs were performed with the SANDER module of the AMBER 6.0 program (*19*), using the all-atom parm94 force field (*20*). Since the pH at which the NMR structures of the salt-bridged form were obtained is 4.5, Arg^{-1}, Lys^{-2}, and Lys^9 residues were protonated and Asp^8 and Glu^{10} residues were deprotonated. His^{16} was protonated at the N$^{\delta 1}$ position. During the molecular dynamics runs, the covalent bond lengths were kept constant by applying the SHAKE algorithm (*24*), allowing a 1.5 fs time step to be used. Coordinates were saved every 1.5 ps. Analyses of the trajectories were performed with the CARNAL module of the AMBER 6.0 suite.

Implicit Solvation. The NMR structures were first minimized for 5000 steps without the NMR constraints to avoid unrealistic drift at the beginning of the molecular dynamics run. All intramolecular noncovalent interactions were computed by setting the nonbonded cutoff at 99 Å. The generalized Born model was used to compute the polar contribution to the solvation free energy, using the parameters from Tsui and Case (*22*). The nonpolar contribution to the solvation free energy was computed as surften × SA, where surften is a surface tension of 0.005 kcal mol^{-1} Å^{-2} and SA is the accessible surface area. The system was coupled to a heat bath with a temperature T_0 of 298 K (*25*), using a temperature relaxation time t_T of 0.2 ps.

Explicit Solvation and Particle-Mesh Ewald Method. Each molecule was immersed in a box of TIP3P water molecules (*26*), and the net charge of the protein was neutralized by substitution of three water molecules for chloride ions. Water molecules with the oxygen atom closer than 2.40 Å or a hydrogen atom closer than 1.80 Å from any protein atom were discarded. The minimum distance from any protein atom and a box edge was 15 Å, resulting in a box containing 4600 water molecules and with initial dimensions of 59 Å × 60 Å × 52 Å. Periodic boundary conditions were imposed in all three dimensions. The system was coupled to a heat bath with a temperature T_0 of 298 K and to a pressure bath with a pressure P_0 of 1 atm by applying the algorithm of Berendsen (*25*). A temperature relaxation time t_T of 1 ps and a pressure relaxation time t_P of 0.2 ps were used, and the pressure scaling was anisotropic. A 500 ps MD simulation in which the protein is kept frozen is performed to equilibrate water molecules and the chloride ions. Then, electrostatic interactions were calculated using the particle-mesh Ewald (PME) summation scheme (*27*), with a cutoff of 10 Å for the separation of the direct and reciprocal space summation and for computation of van der Waals interactions.

RESULTS AND DISCUSSION

We previously showed that N-terminal extension of endothelin-1 (*1*, *3*) or sarafotoxin-S6b (*8*) with the Lys-Arg dipeptide resulted in apparition of pH-dependent conformational changes. Structural studies of these compounds and of analogues indicated that, in their carboxylate state, a salt bridge between Arg^{-1} and Asp^8 probably exists. This salt bridge was deduced from typical chemical shift modification, although no direct observation of this salt bridge could be

afforded by the NMR studies (Figure 2). Indeed, either the proton−proton distances between Arg^{-1} and the Asp^8 side chain were too large to be observed as NOEs, or protons were in fast exchange, as in the guanidinium group. Moreover, formation of the salt bridge displayed an apparent cooperativity with the N-capping of the helix (residues 9−16) by the Asp^8 side chain. We therefore speculated that a synergic effect of helix capping by Asp^8, hydrophobic interactions of Arg^{-1} side chain methylenes with the disulfide bridges, and the Arg^{-1}−Asp^8 salt bridge altogether participate in providing a peculiar stability to the salt-bridged conformation (*8*) (Figure 2). This would be consistent with recent analyses regarding the controversial stability of surface salt bridges. Strop and Mayo suggested that forming solvent-exposed salt bridges may not be favorable because two charges have to be desolvated and immobilized. Stable salt bridges would therefore involve already immobilized charges, thus reducing entropic loss, as in ion pair networks or ion pairs involving charges at the N- or C-terminus (*11*). On the other hand, Takano et al. (*10*) showed that the contribution of surface salt bridges to protein conformational stability is strongly correlated to accessible surface areas of the salt bridge atoms, and can reach 9 kJ/mol for 100% inaccessible atoms. This surface effect was attributed to variations of the dielectric constant that is greatly different between the inside and the outside of a protein.

In KR-ET-1 and KR-SRTb, it was postulated that helix capping strongly reduces the entropy of the Asp^8 side chain and that side chain atoms of Arg^{-1} are significantly involved in hydrophobic interactions with the two disulfide bridges and the Phe^{14} side chain, both effects acting cooperatively to increase the favorable contribution of the Arg^{-1}−Asp^8 salt bridge to the stability of the carboxylate state conformation (*1*, *8*).

Unexpectedly, however, the short molecular simulations performed during the course of these studies did not fully support the stabilizing contribution of the postulated salt bridge that was inferred from the experimental data. This prompted us to synthesize shorter peptides more amenable to detailed simulations studies. Endothelin-1 and sarafotoxin-S6b contain a poorly defined C-terminal tail (residues 17−21) that might not be significantly involved in the pH-dependent conformational changes. These residues were removed from ET-1, yielding a 16-residue peptide hereafter called CSH-ET since it only contains the elementary cystine-stabilized helical motif (*5*, *7*). The corresponding 18-residue peptide with the Lys-Arg N-terminal peptide extension is called KR-CSH-ET. The peptides were amidated at the new C-terminus to avoid introduction of a negative charge at a position where the parent peptide displays a peptide bond.

CD and NMR Data of CSH-ET and KR-CSH-ET Suggest Conformational Behaviors Similar to Those of ET-1 and KR-ET-1. CD spectra of CSH-ET and KR-CSH-ET were recorded at pH 1.5 and 4.0 to track the conformational changes between the carboxylic acid and the carboxylate states previously observed in KR-ET-1 and KR-SRTb. At pH 1.5, CD spectra of CSH-ET and KR-CSH-ET were similar, with an absorption minimum around 206−207 nm. At pH 4.0, the CD spectrum of CSH-ET remained unchanged, whereas the spectrum of KR-CSH-ET was modified and displayed an absorption at 221 nm, suggesting higher helical content. Clearly, the shortened CSH-ET and KR-CSH-ET peptides display the same behavior as ET-1 and KR-ET-1, respectively (*1*−*3*).

Table 1: Ratios of Native to Non-Native Disulfide Bond Isomers Measured in the Oxidative Folding of CSH-ET and KR-CSH-ET in the Presence or in the Absence of the Redox Couple GSH/GSSG, with and without Denaturant

	native to non-native isomer ratios (%)[a]		
	without	with GSH/GSSG	
peptide	GSH/GSSG	without GdnHCl	with GdnHCl[b]
CSH-ET	67/33	65/35	66/34
KR-CSH-ET	96/4	99/1	66/34

[a] The percentage of each isomer was determined by integration of the corresponding HPLC areas. [b] At 6 M.

These results are reinforced by the analysis of disulfide bridge formation during oxidative folding (Table 1). Clearly, the native to non-native ratios for CSH-ET and KR-CSH-ET are similar to those observed for ET-1 and KR-ET-1 (*2*). Thus, analyses of CD spectra and oxidative folding experiments support the hypothesis that the five-residue C-terminal tail present in KR-ET-1 or KR-SRTb is not significantly involved in the pH-dependent conformational changes, and that KR-CSH-ET is an appropriate model for further investigation of this conformational change. ^{1}H NMR spectra of CSH-ET are essentially independent of pH and are not discussed further. In contrast, ^{1}H NMR spectra of KR-CSH-ET in the pH range of 1.75−4.57 fully confirm that KR-CSH-ET undergoes pH-dependent conformational changes very similar to those previously observed in KR-ET-1 and KR-SRTb. Typical chemical shifts of the salt-bridged and salt bridge-free conformations were observed in KR-CSH-ET spectra at pH 4.57 and 1.75, respectively (Figure 4). As previously observed in KR-ET-1, the main chemical shift alterations in the carboxylate state of KR-CSH-ET are a large downfield shift of the Arg^{-1} H^{ϵ} proton (8.80 ppm at pH 4.57 and 7.10 ppm at pH 1.75), a strong nonequivalence of the two H^{δ} protons of Arg^{-1} and of the two H^{β} protons of Asp^8, and an upfield shift and nonequivalence of the aromatic protons of Phe^{14}. It is worth noting that a large downfield shift of the arginine H^{ϵ} proton is an indicator of the formation of a hydrogen-bonded salt bridge in solution (*4*). The amide proton of Asp^8 which is involved in salt bridge formation is also sensitive to pH variations (7.02 ppm at pH 4.57 and 7.85 ppm at pH 1.75).

The Solution Structures of KR-CSH-ET and KR-ET-1 Are Similar. The high degree of similarity between the CD and one-dimensional ^{1}H NMR spectra of KR-CSH-ET at pH $>$4.0 and those of KR-ET-1 and KR-SRTb under the same conditions, as well as the similar pH-dependent behavior, strongly suggest that, when carboxylic acids are deprotonated, KR-CSH-ET displays a three-dimensional salt-bridged conformation very similar to those of KR-ET-1 and KR-SRTb. In the carboxylate form, NOEs between the Arg^{-1} H^{γ} proton and Cys^{11} and Phe^{14} protons are observed in KR-CSH-ET and were previously observed in KR-ET-1 (*1*) and in KR-SRTb (*8*). Also, in the carboxylate form, the two Asp^8 H^{β} protons are strongly nonequivalent (3.52 and 2.60 ppm) with an Asp^8 χ_1 angle near 180°, whereas they are almost equivalent in the carboxylic form. The chemical shifts of the CSH-ET and KR-CSH-ET peptides are available as Supporting Information.

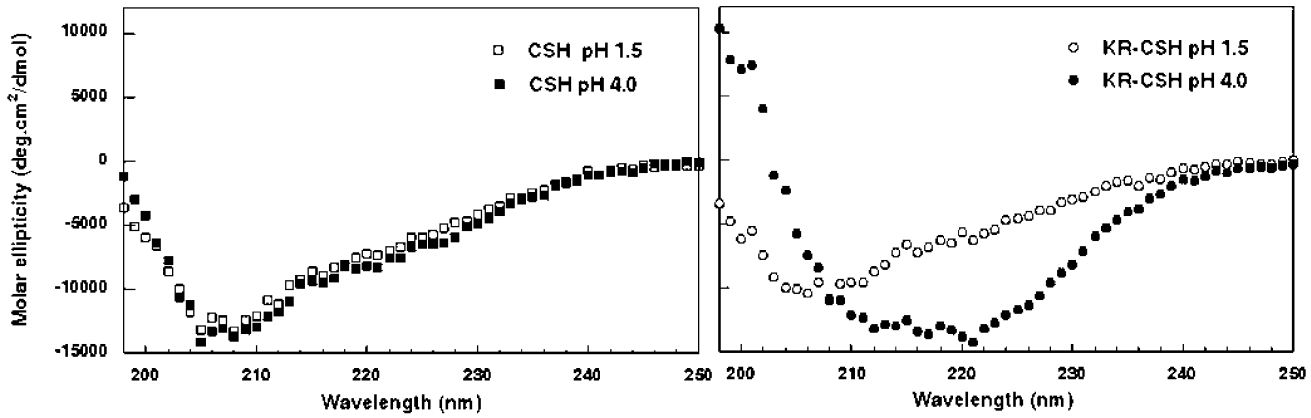

FIGURE 3: CD spectra of the CSH-ET and KR-CSH-ET peptides recorded at pH 1.5 and 4.0.

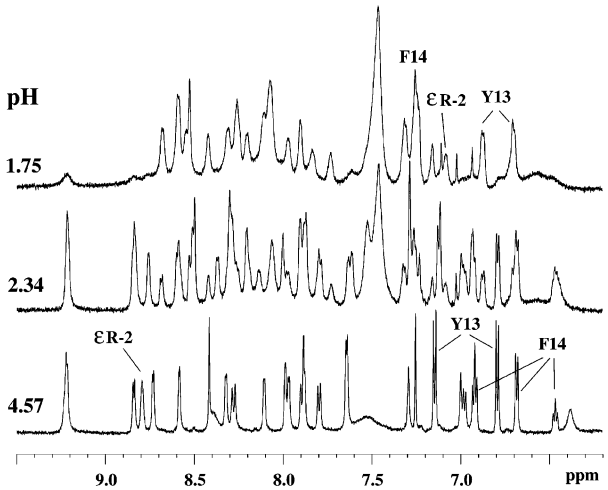

FIGURE 4: Low field area of the KR-CSH-ET spectra recorded at 27 °C in the pH range of 1.75−4.57. For the sake of clarity, only three spectra are displayed. The pH 2.34 spectrum simultaneously shows the typical signals of the two conformations present in the pH 4.57 and 1.75 spectra. Notice that at the latter pH, the extent of line broadening is strongly reduced at lower temperatures and moreover that typical signals of the carboxylate state conformation become observable, since it is the most stable conformation. These changes as a function of temperature support the suggestion that the line broadening is mainly due to the conformational exchange between the major salt bridge-free and the minor salt-bridged conformations (data not shown).

Distance geometry calculations of KR-CSH-ET in the carboxylate state were carried out on the basis of NMR-derived distance constraints and $^3J_{HN-C^\alpha H}$ coupling constants. However, standard NMR methods cannot provide constraints explicitly accounting for the Arg^{-1}−Asp^8 salt bridge (*4*): (i) The H^η protons of Arg^{-1} are exchanged and are not detected, and (ii) all other protons of the Arg side chain are farther than 0.45 nm from Asp side chain protons, precluding the observation of an NOE between Asp and Arg side chains. This was checked for the six representative Arg-Asp conformations in the atlas of protein side chain interactions (http://www.biochem.ucl.ac.uk/bsm/sidechains). Thus, to maintain the Arg^{-1}−Asp^8 salt bridge inferred from NMR data, a distance constraint of 0.5 nm between the Asp^8 Cγ and Arg^{-1} Cζ atoms (*28*) was explicitly added in the calculations. This constraint is loose enough to allow any Arg^{-1}−Asp^8 salt bridge interaction to occur since the corresponding distances measured in the six representative conformations of the atlas of protein side chain interactions lie between 0.42 and 0.47 nm. Moreover, this artificial constraint appeared to be compatible with the NMR constraints because its introduction did not result in any increase in constraint violations. The program DYANA (*18*) was used to compute 1000 conformations that were compatible with the constraints. Using AMBER 6.0 (*19*), the 50 best resulting models were further refined using a molecular dynamics simulated annealing protocol. Refinements in previous studies used either minimization in a shell of water (*8*) or in vacuo molecular dynamics simulated annealing using a distance-dependent dielectric to implicitly take into account the solvent screening (*1*). The generalized Born/surface area (GB/SA) implicit solvation model (*22*, *23*), recently made available in AMBER 6.0, was used in this study since the AMBER−GB/SA combination appeared to be well-suited to refinement of solution structures (*29*). The resulting structures are shown in Figure 5. The mean maximum residual violation is 0.024 nm (SD of 0.002), and the mean number of violations larger than 0.02 nm is 2.2 (SD of 0.9). The mean rms deviation between structures is 0.048 nm (backbone atoms) and 0.128 nm (all heavy atoms).

The amount (%) of accessible surface areas of Arg^{-1} and Asp^8 atoms in the NMR structures compared to that in the denaturated state was calculated for five representative structures selected using the Cluster command in MOLMOL 2K.1 (*16*). For the five structures, the mean ASA (%) value is 50.3 (SD of 1.5), a value that corresponds to a contribution to the conformational stability of 1 kcal/mol according to Takano et al. (*10*).

Finally, all experimental data indicate that KR-CSH-ET displays a pH-dependent conformational change with a conformation in the carboxylate state that is very similar to those of the parent peptide KR-ET-1 and of the chimeric peptide KR-SRTb. This result clearly shows that the pH-dependent conformational change is independent of the C-terminal tail in ET-1. Since it is also independent of the sequence of the loop comprising residues 5−7 (*8*), the conformational change appears to be specific for the KR-CSH elementary motif. Thus, KR-CSH-ET approximately corresponds to the minimum salt-bridged stabilized CSH peptide and should therefore be attractive as a stable elementary scaffold for protein engineering.

Since KR-CSH-ET displays a salt-bridged conformation very similar to those of KR-ET-1 and KR-SRTb, this short and structured peptide also appears to be a good model for simulations of the salt-bridged conformation.

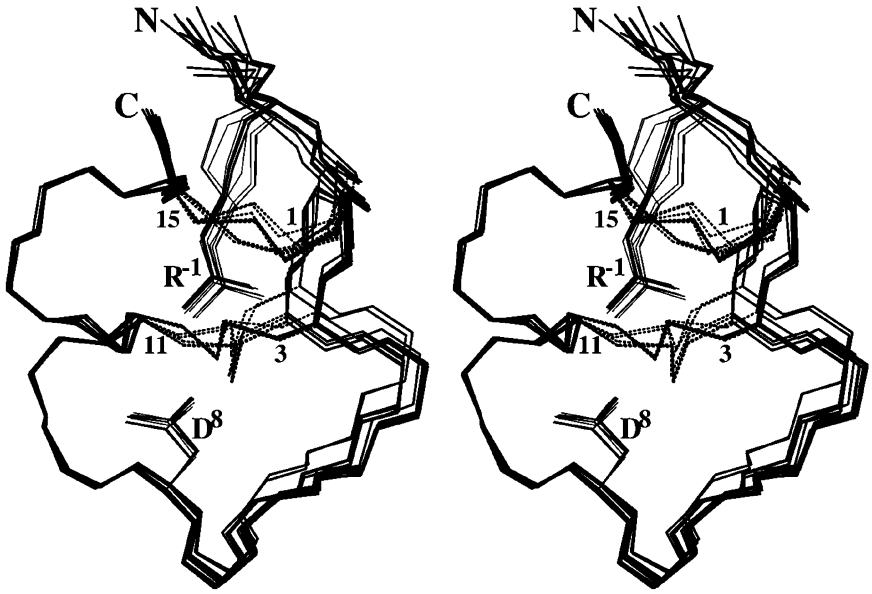

FIGURE 5: Stereoview of 10 calculated solution structures of KR-CSH-ET at pH 4.5. Structures were superimposed for backbone atoms of residues 1−15. Backbones are shown as thick lines. Side chains of Arg^{-1} and Asp^{8} are displayed as thin lines, and disulfide bridges are shown as dotted lines. Arg^{-1} and Asp^{8} side chains are labeled, and cysteines are numbered.

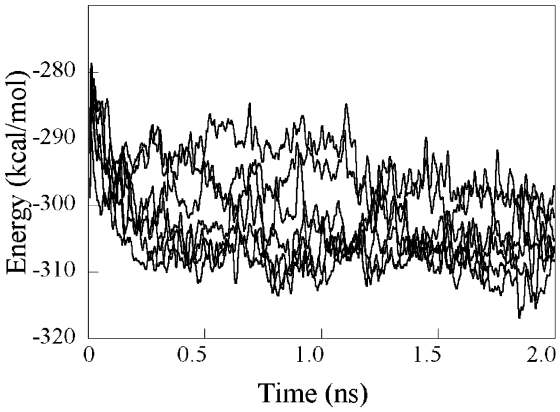

FIGURE 6: Total energy of the KR-CSH-ET peptide in the seven GB/SA simulations.

The Arg^{-1}−Asp^{8} Salt Bridge in Not Maintained in MD Simulations with Implicit Solvation. Explicit inclusion of water molecules in molecular dynamics simulations dramatically increases the size and computational expense of the calculations. Moreover, sampling of the potential energy surface is slowed due to the viscosity of the solvent. More computationally efficient methods have therefore been developed that use implicit solvation models (*21*, *30*−*32*). The generalized Born/surface area (GB/SA) model first introduced by Still and co-workers (*33*, *34*) has recently given excellent results in combination with the AMBER force field (*22*, *23*, *29*, *35*) and was therefore used in this study.

Seven NMR structures with the lowest molecular mechanics energies were submitted to 2 ns simulations, and the corresponding simulations are noted GB/SA-1 to GB/SA-7. As shown in Figures 6 and 7, the mean energies in the simulations are significantly lower than the energies of starting NMR conformations (by ∼10−30 kcal/mol). This was not expected since the NMR structures were refined using the same force field and the GB/SA solvation scheme. The energy decrease is most likely a result of the removal of all NMR constraints, indicating that the conformations calculated with the NMR constraints do not correspond to a true energy minimum. Accordingly, all structures in the simulations deviate significantly from the starting conforma-

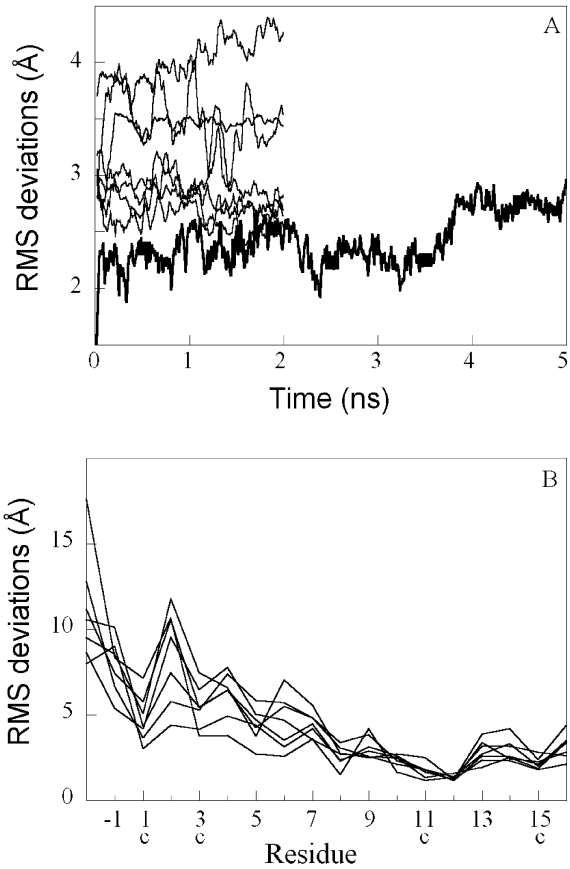

FIGURE 7: (A) rms deviations of the backbone atoms of KR-CSH-ET from their positions in the starting conformations: thin lines, 2 ns GB/SA simulations; and thick line, 5 ns explicit solvent simulation. (B) Mean per-residue rms deviations from the starting conformations as a function of residue number. Conformations of the GB/SA simulations were previously superimposed onto the starting conformation for helical residues 9−15. Values are for all heavy atoms. The letters "c" at the bottom indicate the location of the cysteines.

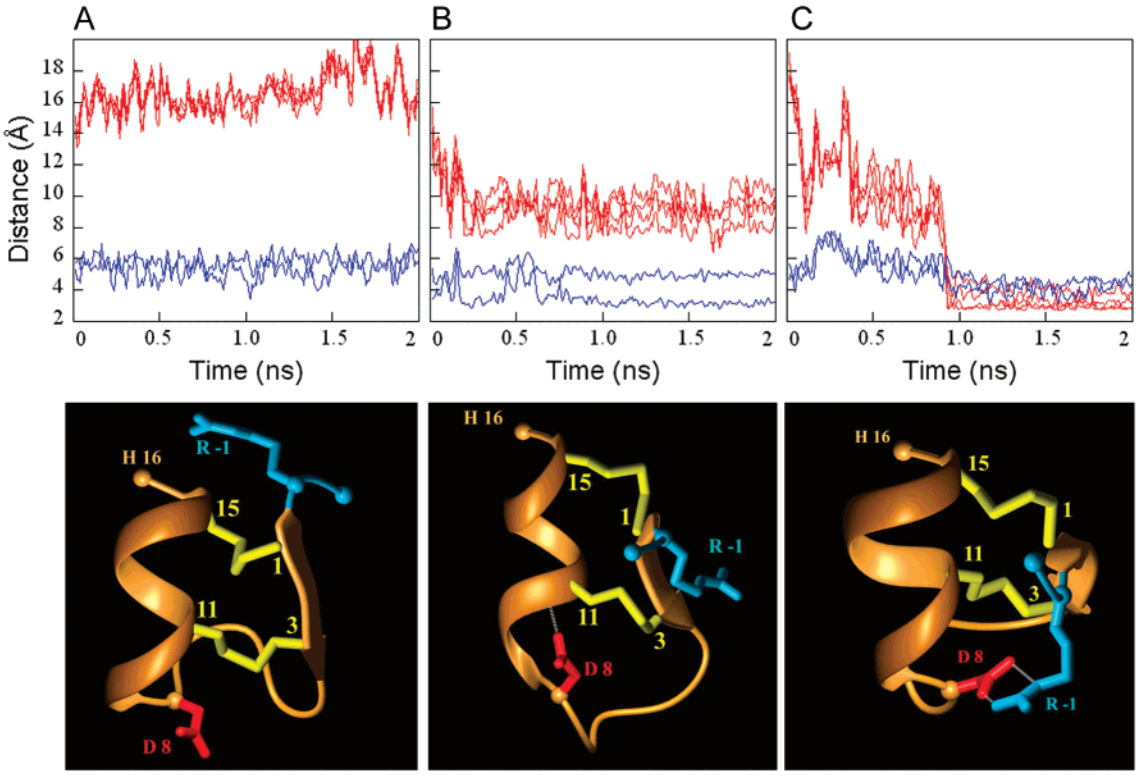

FIGURE 8: (Top) Arg^{-1}—Asp^{8} salt bridge (red, four lines) and Asp^{-8}—Cys^{11} helix capping (blue, two lines) monitored via N—O distances. For the sake of clarity, distances were smoothed over a 15 ps window. (Bottom) Schematic drawing of a representative conformation below each graph. The structures have not been energy minimized. Colors and labels are identical to those in Figure 2. (A) GB/SA-1 simulation with no capping and no salt bridge. The GB/SA-2 and -3 simulations display similar behaviors. (B) GB/SA-4 simulation with capping and no salt bridge. The GB/SA-5 simulation displays similar behavior. (C) GB/SA-6 simulation with no capping and with a salt bridge. The GB/SA-7 simulation displays similar behavior.

tions with rms deviations not lower than 2.5 Å and as high as 4.5 Å. Clearly, although the global CSH fold is maintained in all simulations, the structures undergo significant conformational changes resulting in lower energies. Per-residue rms fluctuations shown in Figure 7B indicate that the largest displacements occur at the N-terminus.

The presence of the Arg^{-1}—Asp^{8} salt bridge and the helix capping by Asp^{8} were monitored via N—O distances between Arg^{-1} and Asp^{8} side chains, and between the Asp^{8} side chain and Cys^{11} backbone amide, respectively. In all seven simulations, both the salt bridge and helix capping, present in the starting NMR structures, were very rapidly lost and corresponding distances cannot be seen in the graphs of Figure 8. From this analysis, the seven GB/SA simulations were grouped into three different types as shown in Figure 8. In Figure 8A (simulation GB/SA-1), all the monitored N—O distances are larger than 4 Å in the simulation. Similar results were obtained for simulations GB/SA-2 and GB/SA-3. In these three simulations, both helix capping and the Arg^{-1}—Asp^{8} salt bridge were rapidly lost during the first few picoseconds and never occur again during the 2 ns long simulations.

In Figure 8B (GB/SA-4 simulation), one capping distance is close to 3 Å. Similar results are observed in the GB/SA-5 simulation. In these two simulations, helix capping is maintained in large parts of the simulations, whereas the Arg^{-1}—Asp^{8} salt bridge is lost. As can be seen in Figure 8C, just the opposite is observed in simulations GB/SA-6 and GB/SA-7.

As can be seen from Figure 8, the previously proposed conformation shown in Figure 1 with both the salt bridge and helix capping appears to be unstable in the simulations since this arrangement, although present in all starting structures, is rapidly lost during the first few picoseconds in all seven simulations. In the two simulations in which the salt bridge reappears part of the time, the conformations display modifications that are not fully consistent with NMR data. First, a large distance between Arg^{-1} and Phe^{14} side chains is observed, although several NOEs indicate their three-dimensional proximity. Second, most salt-bridged conformations display an electrostatic network that also involves the Glu^{10} side chain, in contrast to clear-cut results of mutation experiments which demonstrated the essential role of the Asp^{8} side chain (*2*, *3*).

The fact that simultaneous salt bridge and capping are unstable in the simulations reinforces previous observations that specific constraints were needed to maintain the salt bridge in simulated annealing refinement of NMR structures of KR-ET-1 (*1*) and KR-SRTb (*8*). The instability of the salt-bridged conformation in the GB/SA simulations is particularly surprising since NMR data indicate that this conformation should be largely (>95%) populated (Figure 4). It could be argued that the GB/SA solvation scheme does not adequately reproduce the strength of surface electrostatic interactions. However, a previous in vacuo MD simulation, a condition where electrostatic interactions are largely overestimated, showed that the Arg^{-1}—Asp^{8} interaction is less favored than the Arg^{-1}—Glu^{10} interaction (*1*), although the latter was unambiguously contradicted by subsequent experimental studies of the D8N and E10Q analogues (*2*, *3*).

During the course of these studies, a 200 ps long MD simulation with explicit solvation was also performed. This

short simulation showed a very low level of occurrence (<10%) of the Arg^{-1}−Glu^{10} interaction, and no occurrence of the Arg^{-1}−Asp^{8} interaction.

Finally, all these results seem to converge to indicate that the predicted salt-bridged conformation does not correspond to a particularly stable conformation, since, if particularly stable, it would be significantly populated in the simulations. This observation was further investigated using the more rigorous but computationally extensive method that uses explicit treatment of water molecules and the PME method for calculation of long-range electrostatics. Due to computational limitations, only one 5 ns long simulation was performed.

The Arg^{-1}−Asp^{8} Salt Bridge Is Not Maintained in MD Simulations with Explicit Solvation. Since protein−water and water−water interactions play an essential role in protein folding, the use of explicit water molecules in the simulations, with periodic boundary conditions, appeared to be necessary for obtaining an accurate dynamical description of protein structures. The accuracy of the simulations also strongly depends on the way electrostatic interactions are treated (*36*). Here, the second-generation AMBER force field (*20*) in conjunction with the particle-mesh Ewald method (*27*) was utilized to accommodate the long-range electrostatic interactions. The PME method has been shown to yield results superior to those of standard cutoff methods, generating structures that are more stable, with reduced backbone mobility, and closer to experimental structures (*36*−*38*).

The rms deviation from the initial NMR conformation in the simulation (Figure 7A) remains near 2.2 Å for ∼3 ns, a deviation slightly smaller than deviations obtained in the GB/SA simulations. During the last 2 ns, the deviation increases to ∼2.7 Å. Although these values indicate that the overall structure is retained in the simulation, they are nevertheless larger than classical values for MD simulations of globular proteins in water (*36*). Examination of the structures shows that the N-terminus and the Arg^{-1} side chain mostly deviate from their conformation in the NMR conformer. This is best seen by examination of distances between Arg^{-1} nitrogens and Asp^{8} oxygens that are all larger than 15 Å (Figure 9), although Arg^{-1} and Asp^{8} were involved in a salt bridge in the initial conformation. The Arg^{-1} side chain extends apart from the molecule and remains fully solvated during most of the simulation as in the snapshot shown in Figure 9B. On the other hand, hydrogen bonds related to helix capping show that in the last 2.5 ns of the simulation, helix capping by Asp^{8} is well-established and remains stable (Figure 9), with a restrained rotation of the Asp^{8} side chain (χ_1 angle close to 180°). This is in agreement with the large nonequivalence (0.95 ppm) measured for the two Asp^{8} H^{β} protons in the carboxylate form of KR-CSH-ET. Thus, helix capping, which is remarkably stable in the simulation, strongly restricts the mobility of the Asp^{8} side chain and should help to stabilize the Arg^{-1}−Asp^{8} salt bridge by lowering the entropic cost of salt bridge formation (*11*).

Nevertheless, despite the restricted motion of the Asp^{8} side chain in the simulation, the postulated salt bridge with Arg^{-1} is very rapidly lost and was never formed back in the simulation. As in the implicit solvent simulation, the postulated Arg^{-1}−Asp^{8} salt bridge appears to be unstable in the explicit water simulation also. To check that this result is not specific to the AMBER force field, a short

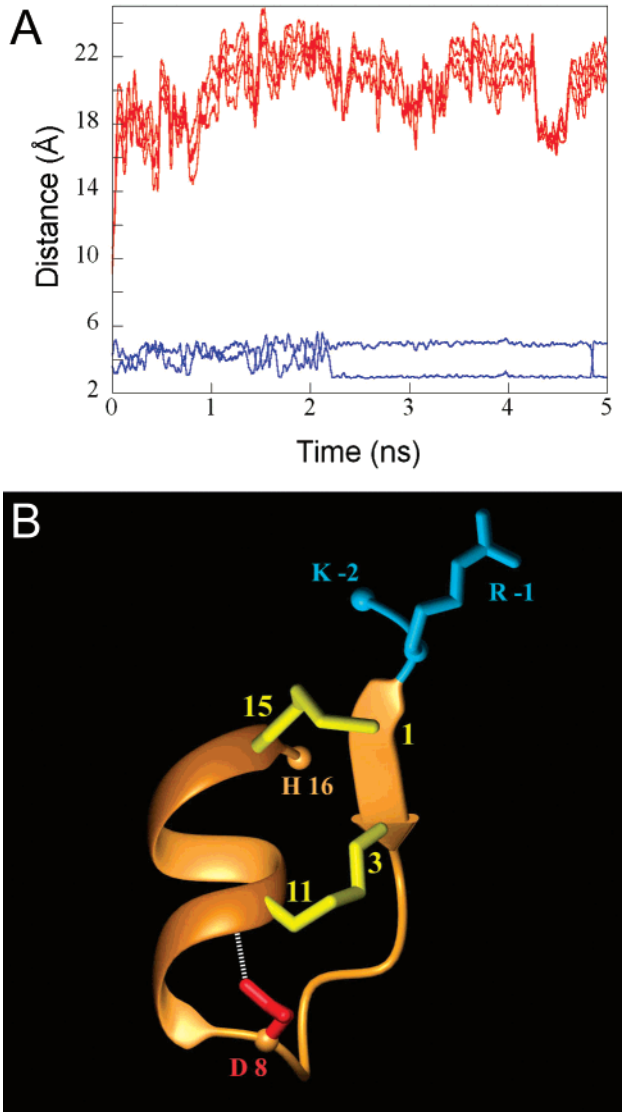

FIGURE 9: (A) Arg^{-1}−Asp^{8} salt bridge (red, four lines) and Asp^{-8}−Cys^{11} helix capping (blue, two lines) monitored via N−O distances in the 5 ns explicit solvent simulation. (B) Schematic drawing of a representative conformation. The structure has not been energy minimized. Colors and labels are identical to those in Figure 2. The K-2 and H16 labels denote the N- and C-termini, respectively.

test simulation (100 ps) in explicit water was performed with the DISCOVER program and the CVFF force field (Accelrys, Inc.). As observed with AMBER, the DISCOVER simulation led to a rapid loss of the Arg^{-1}−Asp^{8} salt bridge. This apparent discrepancy between experiments and simulations could arise from force field difficulties in providing accurate energetics of surface salt bridges due to the subtle balance between protein−protein and protein−water electrostatic interactions. However, recent molecular dynamics simulations, especially those using the PME method to accommodate long-range electrostatic interactions, appeared to display reasonably good accuracy (*36*−*38*). It is worth noting that the Arg^{-1}−Asp^{8} distances are on average larger in the explicit solvent simulation than in all seven GB/SA simulations (compare Figures 8 and 9). From this difference, we conclude that the GB/SA solvation scheme, although much better than in vacuo simulations, still displays a bias that tends to bury the Arg side chain more than the explicit water simulation.

It must be noted that spatial proximities of the H^{ϵ} proton of the Arg^{-1} side chain to Phe^{14} aromatic protons were detected by NMR in the salt-bridged conformations of the three peptides (KR-ET-1, KR-SRTb, and KR-CSH-ET). The close contact between Arg^{-1} and Phe^{14} strongly suggests that a cation$-\pi$ interaction could be cooperatively involved with the $Arg^{-1}-Asp^{8}$ salt bridge in stabilization of the salt-bridged conformation. Cation$-\pi$ interactions involving arginines are common in proteins and can provide significant stabilizing energies (*39*). However, despite the observation that molecular mechanics electrostatic energies of cation$-\pi$ interactions correlate reasonably with the ab initio energy (*39*), the force fields may not be well suited to account for this type of interaction in MD simulations (*9*, *40*). It may then be hypothesized that the $Arg^{-1}-Phe^{14}$ cation$-\pi$ interaction was underestimated in the simulations, thus destabilizing the salt-bridged conformation in the simulations.

It is also worth noting that the conformational exchange between the salt bridge-free conformation and the salt-bridged conformation is slow on the NMR time scale (microseconds to milliseconds), since at intermediate pHs the signals of the two conformations are simultaneously observed in the NMR spectrum (Figure 4). This implies that the conversion between the salt bridge-free conformation and the salt-bridged form is unlikely to happen on the simulation time scale (nanoseconds). It is therefore important that the starting conformation in the simulation be similar to the true salt-bridged conformation. If, however, the salt-bridged conformation corresponds to a very specific side chain arrangement that was missed in the NMR calculation, then MD may also fail to sample this conformation. As an example, we envisaged that a structural water molecule, which would not be seen by NMR, could mediate the specific $Arg^{-1}-Asp^{8}$ interaction. To check this possibility, we manually built a starting model in which one water molecule was inserted between the Arg^{-1} and Asp^{8} side chains. Using this model, a 1 ns long MD simulation was performed under the same conditions used for the explicit water simulation but remained unsuccessful in maintaining the water-bridged $Arg^{-1}-Asp^{8}$ interaction (data not shown).

CONCLUSION

The KR-ET-1 and KR-SRTb peptides, obtained by N-terminal addition of the Arg-Lys dipeptide to endothelin-1 and sarafotoxin-S6b, respectively, display significant conformational modification in the pH range of 1.5−4.5. NMR structural experiments on these peptides and on analogues indicated that the pH-mediated modifications are related to formation of a salt bridge between residues Arg^{-1} and Asp^{8}. The stabilization afforded by this salt bridge was also shown to improve formation of the nativelike disulfide bonds during the oxidative folding of these compounds. Here, we have shown that very similar results are obtained from the shorter KR-CSH-ET peptide that corresponds to the core of KR-ET-1 after removal of the mobile and hydrophobic C-terminal tail. We have thus unambiguously shown that the C-terminal tail is not involved in salt bridge stabilization of the CSH motif. The KR-CSH-ET peptide therefore appears to be an attractive elementary scaffold for drug design. The peptide is easy to synthesize and stable, and moreover, the loop of residues 4−7 displays an interesting sequence permissiveness that suggests potential abilities to present various antigenic or inhibitory sequences.

In all three peptides studied so far that include the N-terminal Lys-Arg dipeptide extension (KR-ET-1, KR-SRTb, and KR-CSH-ET), an $Arg^{-1}-Asp^{8}$ salt-bridged conformation appeared to be highly populated both in NMR and in CD spectra at pH >4, and sufficiently stable to thermodynamically drive disulfide bridges toward their native connectivity. Unexpectedly, however, this conformation displayed some instability in earlier molecular dynamics structure refinements and simulations performed on KR-ET-1 and KR-SRTb. In this work, more accurate molecular dynamics simulations have been performed on the shorter peptide, KR-CSH-ET. The simulations were conducted using both the GB/SA implicit solvation scheme or with explicit solvation and the PME method for long-range electrostatic calculation, and clearly show that the postulated $Arg^{-1}-Asp^{8}$ salt bridge does not display, in the simulation, the stability that could be inferred from the experimental data. Whether this is due to a deficiency of the MD calculations, or to partial misinterpretation of experimental data due to the occurrence of a special and unexpected phenomenon, remains to be determined.

At this time, no satisfactory explanation for the discrepancy between experiments and simulations is available, and further experimental studies appear to be necessary to fully understand in atomic detail the pH-dependent conformational change observed in the KR-ET-1 series. This is highly desirable for at least two reasons. First, molecular dynamics simulation is at present a widely used tool, and any possible pitfalls should be highlighted, such as, for example, limited accuracy in accounting for cation$-\pi$ interactions. Second, the stabilized KR-CSH-ET structural motif presented here should find useful applications as an elementary scaffold in drug design and protein engineering. As an example of possible future work, we plan to experimentally check the impact of the putative $Arg^{-1}-Phe^{14}$ cation$-\pi$ interaction on the stability of the salt-bridged conformation at pH 4, by replacing Phe^{14} in KR-CSH-ET with a nonaromatic hydrophobic residue such as Leu or Ile. Direct observation of the $Arg^{-1}-Asp^{8}$ hydrogen bonding interaction in solution would, in principle, also be possible by using the costly $^{13}C-^{15}N$ double labeling of Arg^{-1} and Asp^{8} residues along with the new NMR methodology (*4*).

ACKNOWLEDGMENT

We thank Amelie Dreux for help in NMR assignments and calculations.

SUPPORTING INFORMATION AVAILABLE

NMR data for the KR-CSH-ET peptide in water and the CSH-ET peptide in water. This material is available free of charge via the Internet at http://pubs.acs.org.

REFERENCES

1. Aumelas, A., Chiche, L., Kubo, S., Chino, N., Tamaoki, H., and Kobayashi, Y. (1995) *Biochemistry 34*, 4546−4561.
2. Kubo, S., Chino, N., Nakajima, K., Aumelas, A., Chiche, L., Segawa, S., Tamaoki, H., Kobayashi, Y., Kimura, T., and Sakakibara, S. (1997) *Lett. Pept. Sci. 4*, 185−192.
3. Aumelas, A., Kubo, S., Chino, N., Chiche, L., Forest, E., Roumestand, C., and Kobayashi, Y. (1998) *Biochemistry 37*, 5220−5230.

4. Liu, A., Hu, W., Majumdar, A., Rosen, M. K., and Patel, D. J. (2000) *J. Biomol. NMR 17*, 305−310.
5. Tamaoki, H., Miura, R., Kusunoki, M., Kyogoku, Y., Kobayashi, Y., and Moroder, L. (1998) *Protein Eng. 11*, 649−659.
6. Tamaoki, H., Kyogoku, Y., Nakajima, K., Sakakibara, S., Hayashi, M., and Kobayashi, Y. (1992) *Biopolymers 32*, 353−357.
7. Kobayashi, Y., Takashima, H., Tamaoki, H., Kyogoku, Y., Lambert, P., Kuroda, H., Chino, N., Watanabe, T. X., Kimura, T., Sakakibara, S., et al. (1991) *Biopolymers 31*, 1213−1220.
8. Aumelas, A., Chiche, L., Kubo, S., Chino, N., Watanabe, T. X., and Kobayashi, Y. (1999) *Eur. J. Biochem. 266*, 977−985.
9. Iurcu-Mustata, G., Van Belle, D., Wintjens, R., Prevost, M., and Rooman, M. (2001) *Biopolymers 59*, 145−159.
10. Takano, K., Tsuchimori, K., Yamagata, Y., and Yutani, K. (2000) *Biochemistry 39*, 12375−12381.
11. Strop, P., and Mayo, S. L. (2000) *Biochemistry 39*, 1251−1255.
12. Loladze, V. V., and Makhatadze, G. I. (2002) *Protein Sci. 11*, 174−177.
13. Kumagaye, S., Kuroda, H., Nakajima, K., Watanabe, T. X., Kimura, T., Masaki, T., and Sakakibara, S. (1988) *Int. J. Pept. Protein Res. 32*, 519−526.
14. Nakajima, K., Kubo, S., Kumagaye, S., Nishio, H., Tsunemi, M., Inui, T., Kuroda, H., Chino, N., Watanabe, T. X., Kimura, T., et al. (1989) *Biochem. Biophys. Res. Commun. 163*, 424−429.
15. Plateau, P., and Guéron, M. (1982) *J. Am. Chem. Soc. 104*, 7310−7311.
16. Koradi, R., Billeter, M., and Wuthrich, K. (1996) *J. Mol. Graphics 14*, 51−55.
17. Wüthrich, K., Billeter, M., and Braun, W. (1983) *J. Mol. Biol. 169*, 949−961.
18. Guntert, P., Mumenthaler, C., and Wuthrich, K. (1997) *J. Mol. Biol. 273*, 283−298.
19. Case, D. A., Pearlman, D. A., Caldwell, J. W., Cheatham, T. E., Ross, W. S., Simmerling, C. L., Darden, T. A., Merz, K. M., Stanton, R. V., Cheng, A. L., Vincent, J. J., Crowley, M., Tsui, V., Radmer, R. J., Duan, Y., Pitera, J., Massova, I., Seibel, G. L., Singh, U. C., Weiner, P. K., and Kollman, P. A. (1999) *AMBER 6.0*, University of California, San Francisco.
20. Cornell, W. D., Cieplak, P., Bayly, C. I., Gould, I. R., Merz, K. M., Jr., Ferguson, D. M., Spellmeyer, D. C., Fox, T., Caldwell, J. W., and Kollman, P. A. (1995) *J. Am. Chem. Soc. 117*, 5179−5197.
21. Bashford, D., and Case, D. A. (2000) *Annu. Rev. Phys. Chem. 51*, 129−152.
22. Tsui, V., and Case, D. A. (2000) *J. Am. Chem. Soc. 122*, 2489−2498.
23. Cornell, W., Abseher, R., Nilges, M., and Case, D. A. (2001) *J. Mol. Graphics Modell. 19*, 136−145.
24. van Gunsteren, W. F., and Berendsen, H. J. C. (1977) *Mol. Phys. 34*, 1311−1327.
25. Berendsen, H. J. C., Postma, J. P. M., van Gunsteren, W. F., DiNola, A., and Haak, J. R. (1984) *J. Chem. Phys. 81*, 3684−3690.
26. Jorgensen, W. L., Chandreskhar, J., Madura, J. D., Imprey, R. W., and Klein, M. L. (1983) *J. Chem. Phys. 79*, 926−935.
27. Darden, T. A., York, D., and Pedersen, L. (1993) *J. Chem. Phys. 98*, 10089.
28. Creighton, T. E. (1993) *Proteins, Structures and Molecular Properties*, 2nd ed., p 143, W. H. Freeman, New York.
29. Heitz, A., Hernandez, J. F., Gagnon, J., Hong, T. T., Pham, T. T., Nguyen, T. M., Le-Nguyen, D., and Chiche, L. (2001) *Biochemistry 40*, 7973−7983.
30. Simonson, T. (2001) *Curr. Opin. Struct. Biol. 11*, 243−252.
31. Lazaridis, T., and Karplus, M. (2000) *Curr. Opin. Struct. Biol. 10*, 139−145.
32. Kollman, P. A., Massova, I., Reyes, C., Kuhn, B., Huo, S., Chong, L., Lee, M., Lee, T., Duan, Y., Wang, W., Donini, O., Cieplak, P., Srinivasan, J., Case, D. A., and Cheatham, T. E., III (2000) *Acc. Chem. Res. 33*, 889−897.
33. Qiu, D., Shenkin, P. S., Hollinger, F. P., and Still, W. C. (1997) *J. Phys. Chem. A 101*, 3005−3014.
34. Still, W. C., Tempczyk, A., Hawley, R., and Hendrickson, T. (1990) *J. Am. Chem. Soc. 112*, 6127−6129.
35. Cheatham, T. E., III, Srinivasan, J., Case, D. A., and Kollman, P. A. (1998) *J. Biomol. Struct. Dyn. 16*, 265−280.
36. Fox, T., and Kollman, P. A. (1996) *Proteins 25*, 315−334.
37. Norberto de Souza, O., and Ornstein, R. L. (1999) *J. Biomol. Struct. Dyn. 16*, 1205−1218.
38. Zuegg, J., and Gready, J. E. (1999) *Biochemistry 38*, 13862−13876.
39. Gallivan, J. P., and Dougherty, D. A. (1999) *Proc. Natl. Acad. Sci. U.S.A. 96*, 9459−9464.
40. Wintjens, R., Lievin, J., Rooman, M., and Buisine, E. (2000) *J. Mol. Biol. 302*, 395−410.

BI025744Z